ACS APPLIED MATERIALS & INTERFACES

www.acsami.org

Research Article

Nontoxic Liquid-Infused Slippery Coating Prepared on Steel Substrates Inhibits Corrosion and Biofouling Adhesion

Alexander B. Tesler,* Lucia H. Prado, Ingo Thievessen, Anca Mazare, Patrik Schmuki, Sannakaisa Virtanen, and Wolfgang H. Goldmann*

Cite This: *ACS Appl. Mater. Interfaces* 2022, 14, 29386–29397

Read Online

ACCESS | Metrics & More | Article Recommendations | Supporting Information

ABSTRACT: Wetting of surfaces plays a vital role in many biological and industrial processes. There are several phenomena closely related to wetting such as biofouling and corrosion that cause the deterioration of materials, while the efforts to prevent the degradation of surface functionality have spread over several millennia. Antifouling coatings have been developed to prevent/delay both corrosion and biofouling, but the problems remain unsolved, influencing the everyday life of the modern society in terms of safety and expenses. In this study, liquid-infused slippery surfaces (LISSs), a recently developed nontoxic repellent technology, that is, a flat variation of omniphobic slippery liquid-infused porous surfaces (SLIPSs), were studied for their anti-corrosion and marine anti-biofouling characteristics on metallic substrates under damaged and plain undamaged conditions. Austenitic stainless steel was chosen as a model due to its wide application in aquatic environments. Our LISS coating effectively prevents biofouling adhesion and decays corrosion of metallic surfaces even if they are severely damaged. The mechanically robust LISS reported in this study significantly extends the SLIPS technology, prompting their application in the marine environment due to the synergy between the facile fabrication process, rapid binding kinetics, nontoxic, ecofriendly, and low-cost applied materials together with excellent repellent characteristics.

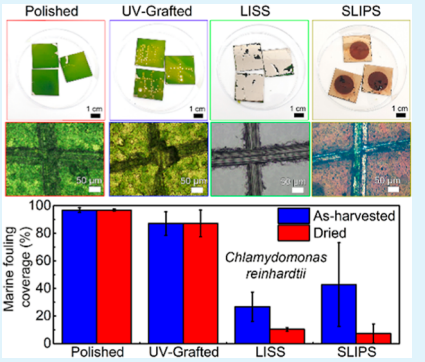

KEYWORDS: *liquid-infused slippery surfaces, polydimethylsiloxane, corrosion resistance, anti-biofouling coating, biofilms, diatoms, algae*

INTRODUCTION

Any surface immersed in water is subjected to the settlement of aquatic organisms, which is called biofouling.[1] Biofouling is a serious and undesirable problem for various industrial sectors and, in particular, maritime ones. It is a worldwide problem involved in almost every water-based process, such as the food industry, potable water storage, cooling towers, heat exchangers, underwater constructions, membrane technology,[2] and ship hulls, causing incredible annual expenses and being responsible for an increase of ~40% emissions of CO_2/SO_2 during transport alone.[3] The direct economic costs of managing biofouling in the aquaculture industry are estimated to be ~10% of production costs, which was around 2.5×10^{11} USD in 2018 and at an annual growth rate of 5.8%.[4]

Biofouling is a multistage process initiated by the formation of a "conditioning layer" of microfoulers, that is, bacteria, diatoms, and/or microalgae.[5] The attached cells adsorb organic molecules on the surface, thus promoting the formation of a biofilm matrix on which multicellular micro- and macrofoulers develop.[6] Since ancient times, anti-biofouling surfaces have been designed to reduce the extent of bacteria attachment and proliferation of biofilms by either killing them locally or slowing down their growth.[7] Antifouling (AF) coatings (mainly paints) have been developed to prevent the attachment of marine organisms. The earliest coatings contained toxic compounds such as arsenic or tin, acting as a broad-spectrum biocide.[5] However, the environmental effects of these compounds became apparent on aquatic life and, more specifically, on non-targeted fouling organisms, which finally led to their ban in 2008.[8] Currently, anti-biofouling coatings involve two main strategies: (i) chemically active biocide coatings based on Cu or Zn, organic complexes, and enzymes, which act on marine organisms,[9] while the release rate of soluble species from AF paints is now regulated in several countries including the US and EU.[8] (ii) Nontoxic AF coatings, which act either to inhibit the settlement of organisms or enhance the release of settled organisms [fouling release (FR)] without involving chemical reactions or toxic chemicals.[5,8,10] The nontoxic AF strategy is inspired by natural organisms such as shark skin[11] or mollusk shells[12] in their defense against biofouling. Several material properties/approaches have been tailored to facilitate a nontoxic, surface-associated FR character such as a low modulus of elasticity, a low surface energy, amphiphilicity, texturing, and

Received: March 20, 2022
Accepted: May 26, 2022
Published: June 13, 2022

https://doi.org/10.1021/acsami.2c04960
ACS Appl. Mater. Interfaces 2022, 14, 29386–29397

so forth to interfere with or stymie organism attachment and interfacial adhesive bonding.[8,13,14] One of the FR strategies is based on minimizing the adhesion between fouling organisms and the surface by introducing additive oil to enhance their slipperiness; hence, fouling can be removed by simple mechanical cleaning such as a water jet or by hydrodynamic stress during the navigation of sea vessels.[8]

During the last decades, several strategies have been developed to combat biofouling. Superhydrophobic surfaces (SHSs), inspired by the lotus leaf architecture, emerged as a potential solution for creating AF surfaces.[15] However, the "Achilles heel" of the SHS is the poor mechanical and pressure stability of the hierarchical micro-/nanoscaled surface topography that is essential for obtaining high water contact angles (WCAs) from one side[16,17] and metastability of the plastron underwater (the thin air film that separates the solid substrate from contact with water) from another side.[18] Although the poor mechanical durability can be improved by structuring surfaces at two different length scales,[19] the restricted underwater plastron stability limits their scope for commercial applications.[18]

Slippery liquid-infused porous surfaces (SLIPSs) have recently been introduced as an alternative approach to the conventional SHS.[20] Inspired by *Nephenthes pitcher*, the slippery surface concept is based on the infusion of a porous substrate with a lubricating fluid that has a strong chemical affinity to the underlying substrate, creating a stable, inert, and extremely smooth lubricant overlayer on the surface. The premise of slippery coatings is that a liquid surface is intrinsically smooth and defect free down to the molecular scale, thus reducing drag and the strength of adhesion of contaminants. SLIPS can function under harsh conditions suitable for a wide range of applications,[20−36] while the major and substantial limitations of the SLIPS approach remain: the mechanical weakness due to the basic requirement for rough/porous surfaces[20] and the numerous steps in the preparation process.[37]

Recently, we have developed a facile one-pot process to alter plain substrates made of metals, metal oxides, ceramics, and silicones into LISSs.[38] No pre- or post-modification treatments are needed to adopt such solid substrates to LISSs in a matter of minutes. The coating consists solely of polydimethylsiloxane (PDMS), the most common silicone material, which is eco-friendly and nontoxic to aquatic life.[39,40] The coating can successfully repel complex fluids such as blood and substantially reduce the attachment of Gram-positive and Gram-negative bacteria. Our LISS substrates are as mechanically robust as their plain counterparts because the procedure does not require any surface structuring, making them advantageous over conventional SLIPS substrates.

In this study, we extend the application of LISS-coating technology by exposing LISS-coated stainless steel substrates to aquatic organisms such as freshwater green algae and seawater diatoms. Although green algal biofilms have proven to be remarkable indicators for the effectiveness of continuous, immobilized lubricant layers, that is, intrinsic characteristics of the slippery surface technology,[27,41,42] diatoms are known as early surface colonizers.[40,43] Here, we demonstrate that LISS, prepared on flat (nonporous) substrates, repels adhesion of such living organisms and inhibits pitting corrosion of steel substrates. Furthermore, we examined the influence of mechanical damage on LISSs on their anti-corrosion and anti-biofouling characteristics. Within the framework of short-term laboratory studies, the performance of damaged LISS surfaces was found comparable to that of SLIPSs, which is the state-of-the-art nontoxic repellent technology, while from the technological/engineering perspective, the preparation of LISS is considerably simpler.

EXPERIMENTAL SECTION

Materials. Stainless steel 316L was purchased from Outokumpu, Finland. Before surface functionalization, the substrates were ultrasonically degreased in acetone and ethanol for 10 min and then dried under a stream of N_2. PDMS (silicone oil), toluene, ethanol, and acetone were purchased from Carl Roth, Germany, and used as received.

Surface Functionalization and Lubrication. Stainless steel AISI 316L cut into 1 × 30 × 30 mm sized specimens were used as substrates. The surface was ground up to 1200 SiC, subsequently polished up to a 1 μm diamond suspension, and cleaned by ultrasonication with acetone and ethanol. The polished samples were horizontally placed in a Petri dish under a quartz cover. Approximately 20 μL cm^{-2} silicone PDMS oil was then pipetted on to cover the entire sample surface, and uniform coverage was achieved by tilting the sample. The samples were illuminated using a medium-pressure ultraviolet (UV) (Hg) lamp at 1 kW (UVAPRINT HPV, Hoenle AG, Germany). The emission maxima of this type of lamp are in the UV range, that is, λ = 320 and 365 nm. The working distance between the lamp and the sample was ∼20 cm. The UV light power density was measured using a 1830-C Newport optical power meter, equipped with an 818-UV/DB optical power detector and a 1% Newport ND filter. The power density at the working distance was ∼100 mW cm^{-2}. For further characterization of the UV-grafted PDMS layers, the remnant oil was dissolved by an extensive rinse in toluene and then dried under a stream of N_2.

Anodization of Stainless Steel to Form SLIPS Samples. The electrochemical anodization was performed in a standard two-electrode cell using a LAB/SM 7300 DC power supply (ET System, Germany), 316L grade stainless steel as an anode, and Pt foil as a cathode. Stainless steel samples were anodized in a two-step procedure as previously reported by us.[44,45] Briefly, an ethylene glycol solution containing 0.1 M of NH_4F and 0.2 M H_2O was used as an electrolyte, and the anodization was performed at 20 °C at an applied potential of 90 V. The first step of anodization was performed for 20 min. Then, the porous anodic layer was removed using a UP100H ultrasonic processor (Hielscher, Germany) in water for 5 min and dried under a stream of N_2. Thereafter, a second anodization step was performed for 10 min in a similar electrolyte. After the second-step anodization, the samples were extensively rinsed with a 20:80 (v/v) water−ethanol mixture, and then kept in ethanol until annealed in air at 400 °C for 1 h.

Freshwater Green Algae Laboratory Assay. The stock solutions of green algae such as *Chlamydomonas reinhardtii* (*C. reinhardtii*, CCAP 11/32B) or *Chlorella sorokiniana* (*C. sorokiniana*, CCAP 211/8K) were purchased from the Scottish Association for Marine Science (CCAP) and used as model organisms to explore the biofilm adhesion on LISS surfaces. *C. reinhardtii* and *C. sorokiniana* were grown in a 3N-BBM+V medium (CCAP FA3N-C) solution under nonaxenic conditions. The stock culture solutions were placed under a fluorescent daylight (Philips TL5HO) fixture and continuously grown at 16 h on and 8 h off light cycles at room temperature (18−20 °C) under rocking conditions.

Seawater Diatom Laboratory Assay. The seawater diatom of the type *Cyclotella cryptica* (*C. cryptica*, CCAP 1070/2) purchased from the Scottish Association for Marine Science (CCAP) was used as a model organism to explore the biofilm adhesion on LISS and control samples. *C. cryptica* was grown in a *f*/2 + Si seawater medium (CCAP MAF2S−C) under nonaxenic conditions. The stock culture solutions were placed under a fluorescent light (Philips TL5HO) fixture at room temperature (18−20 °C) and were continuously grown at 16 on and 8 h off light cycles under rocking conditions. The seawater was prepared according to the following reference.[46]

Contact Angle Measurements. The WCA measurements were performed by a contact angle measuring system (DSA100, Kruss, Germany) at room temperature. The droplet volume for the measurements was 10 μL, unless otherwise specified, and the

https://doi.org/10.1021/acsami.2c04960
ACS Appl. Mater. Interfaces 2022, 14, 29386−29397

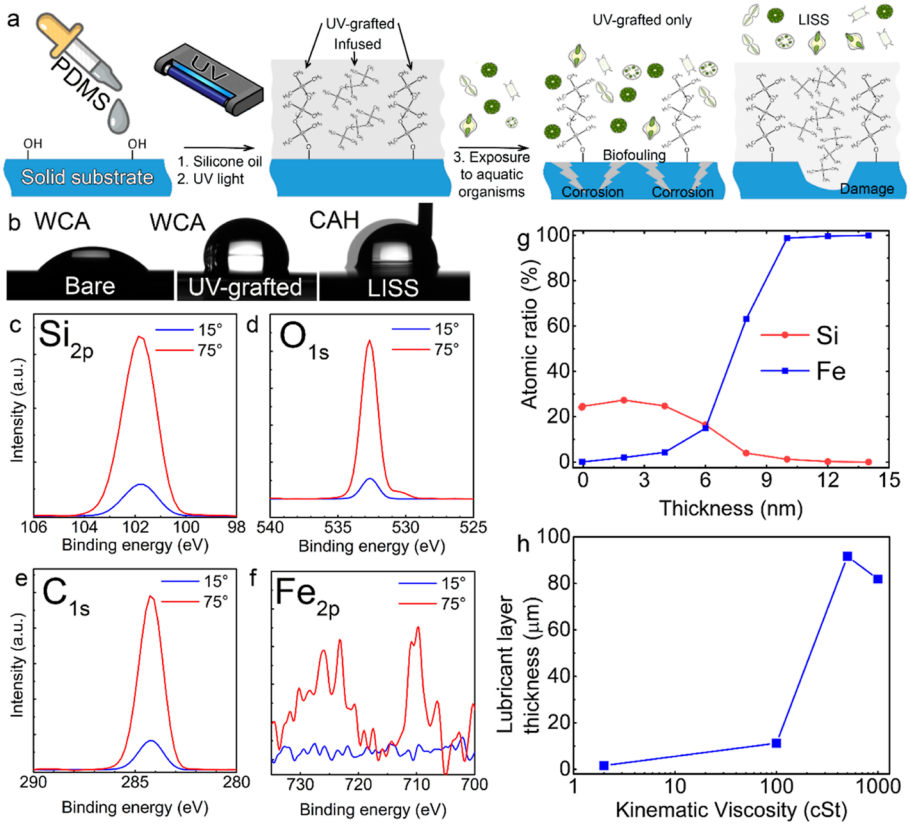

Figure 1. (a) Schematic representation of UV-grafting procedure of PDMS to solid substrates and biofouling experiments. (b) WCA of the cleaned polished stainless steel substrate (left image), the UV-grafted PDMS on the polished stainless steel substrate (middle image), and the WCA and CAH of the LISS PDMS on the polished stainless steel substrate (right image). (c–f) High-resolution angle-resolved XPS spectra of the UV-grafted 500 cSt PDMS oil on polished stainless steel substrates: (c) Si 2p, (d) O 1s, (e) C 1s, and (f) Fe 2p. (g) XPS depth profile of Si and Fe UV-grafted PDMS oil on the polished stainless steel substrate. The unbound PDMS molecules were dissolved in toluene. (h) Lubricant (PDMS) layer thickness was measured on LISS substrates using confocal microscopy imaging.

macroscopic droplet profile was captured on camera. The droplet profile was fitted using a Drop Shape Analysis computer program provided by the manufacturer. Contact angle hysteresis (CAH) was measured by increasing and decreasing the droplet volume and video recordings to determine the advancing and receding contact angles. All the contact angle values specified in the text were averaged by at least three independent measurements.

Open-Circuit Potential and Potentiodynamic Polarization Measurements. Corrosion experiments were performed in a 3.5 wt % NaCl electrolyte with a three-electrode configuration, where the sample was connected as the working electrode, a platinum electrode as a counter electrode, and an Ag/AgCl (3 M KCl) as a reference electrode. The sample was in contact with the solution through a circular O-ring sealed opening in the cell wall, exposing a circular area of 10 mm in diameter in the case of bare and grafted substrates and 20 mm in the case of the LISS sample. For each sample, open-circuit potential (OCP) measurements (Zahner Zennium Electrochemical Workstation) were performed until reaching a stable OCP value; subsequently, a diamond scraper was used to scratch the surface of the substrate. As soon as the OCP measurement was concluded, potentiodynamic polarization was conducted at room temperature at a 3 mV s^{-1} scanning rate, from −300 mV versus OCP until 2 V in the anodic direction.

Morphology and Physicochemical Characterization. For morphological characterization, a field-emission scanning electron microscope (Hitachi FE-SEM S4800) was used, equipped with an energy-dispersive X-ray spectroscope (Genesis, Oxford Instruments). To obtain green algae and diatom images, the scanning electron microscopy (SEM) voltage was adjusted to 2 kV to reduce surface charging. The composition and the chemical state of the films were characterized using X-ray photoelectron spectroscopy (XPS, PHI 5600, US), and the spectra were shifted according to the C 1s signal at 284.8 eV, and the peaks were fitted using MultiPak software. Depth profiling was carried out using the instrument's Ar^+ sputter source operated at 3 kV and 15 nA, rastered over a 3 × 3 mm^2 area at a sputtering angle of 45° to the surface normal. Sputter steps of 1 min were repeated until the Si substrate. The atomic composition was determined between consecutive sputtering intervals by evaluating the photoelectron peak area using MultiPak processing software. The sputtering rate was calibrated using commercial Si/SiO_2 wafers [3 in. Si(100) p-type with 100 nm SiO_2, μChemicals, Germany] and found to be 2 nm min^{-1}. The thickness of the UV-grafted PDMS layers was determined using a phase-modulated ellipsometer equipped with a 633 nm He–Ne laser source (Picometer Ellipsometer; Beaglehole Instruments, New Zealand). To achieve sufficient sensitivity for the detection of thin silicone layers, angle scans were performed around the Brewster angle of Si (i.e., 76°)[47] from 70 to 80° at a step width of 1° at three different positions of the sample surface. Angle-resolved data from ellipsometry were fitted assuming a four-layer model by refractive indices of n_{air} = 1.00, n_{PDMS} = 1.403, n_{SiO_2} = 1.457, n_{Si} = 3.4, and k_{Si} = 0.03 for air, PDMS layers, native silicon oxide, and silicon wafer, respectively, while a plane Si wafer [with a native oxide layer, p-type Si wafer (μChemicals, Germany)] was used as reference.

Algae and Diatom Biofilm Adhesion. Bare polished, PDMS UV-grafted (hydrophobic), LISS, and anodized-porous SLIPS stainless steel samples were placed horizontally in a 10 cm polystyrene Petri dish with three samples of 2 cm^2 each per dish. The freshwater green algae (*C. reinhardtii* or *C. sorokiniana*) and seawater diatom (*C. cryptica*) were used to explore biofilm retention on all the surfaces. The stock solution was diluted 1:5 with the appropriate growth medium. Thereafter, the surface of each sample was covered with ∼80 mL of the aquatic organism solution (approximately 1 cm thick above the substrate

https://doi.org/10.1021/acsami.2c04960
ACS Appl. Mater. Interfaces 2022, 14, 29386–29397

surface). All the samples were incubated at ∼23 °C (room temperature) for 8 days at 16 h/8 h daylight/dark illumination cycles to allow proper biofilm growth. After 8 days, the samples were photographed, then immersed in a large dish of tap water and pulled out of the culture medium at a controlled rate of 0.5 mm s^{-1} using a dip coater (RDC15, Bungard, Germany). The treated substrates were photographed immediately after removal from the culture to avoid biofilm retraction. The images were then analyzed using ImageJ to assess the remaining biofilm coverage after the air−water interface transition. Triplicates were used in all the biofouling experiments. Furthermore, images were captured by confocal microscopy (Leica, Wetzlar, Germany), bright-field optical microscopy (Nikon, Japan), and SEM (Hitachi, Japan) without any additional pre-treatments using a 2 kV working voltage and 10 μA working current.

RESULTS AND DISCUSSION

Figure 1a shows the schematic representation of the LISS substrates prepared by the UV grafting of the PDMS (i.e., silicone oil) process, which were applied to prevent corrosion and repel fouling of aquatic organisms. Previously, LISSs were applied to various ceramic and metallic substrates,[38] while in this study, austenitic stainless steel was chosen as a substrate due to its wide application in marine environments, owing to good corrosion resistance, easy formability, and excellent mechanical properties.[48] The coating was applied on austenitic stainless steel of the AISI 316L grade, utilized in coastal service environments, splash zone applications, and submersion in seawater, to name but a few.[49,50] In this study, the stainless steel substrates were polished before being modified by LISS coating for better color contrast between the substrate and contaminating fouling species, while the same process can be equally applied to plain steel substrates.

These plain polished samples are hydrophilic, displaying a WCA of 47.9° ± 1.1° (Figure 1b, left image). They were placed horizontally in a Pyrex Petri dish, and a thin layer of silicone oil was dropped on the substrates, allowing them to spread over the entire sample surface area (Figure 1a, step 1). The samples were illuminated by UV light for 30 min, resulting in the formation of PDMS LISS substrates (Figure 1a, step 2). In this study, the medium-pressure mercury UV lamp was used to irradiate all the substrates, while the typical spectrum of such lamps is presented in Figure S1, Supporting Information. As shown, two main intensity peaks are observed at λ = 320 and 370 nm. Previously, we demonstrated that the dissociation enthalpy for Si−CH_3 bonds within the PDMS chain is the smallest; therefore, these bonds are generally weaker and more likely to break. UV light of 317 < λ < 321 nm (UVA) is required for the specific photodissociation of trimethylsilyl bonds at the PDMS end groups, while much stronger UV light is needed for Si−O bonds.[38] The latter indicates that the lamp with sufficient energy at λ = 321 nm is required to activate PDMS oil at Si−CH_3 end group bonds, which are grafted to the surfaces via silicon.

The LISS substrates are hydrophobic with a WCA of 106 ± 1° and a WCA hysteresis of 2.6 ± 0.8° (Figure 1b, right image). To study the UV-grafted PDMS layers, the LISS substrates were prepared on a Si wafer. The remnant oil was removed by extensively rinsing it with toluene,[51] followed by a wash in ethanol, and finally dried under a stream of N_2. The UV-grafting reaction yields a 9.4 ± 0.2 nm thick coating on a flat Si wafer measured by ellipsometry for 500 cSt (M_w = 17.3 kDa) silicone oil, corresponding to a grafting density of 2.5 × 10^{17} PDMS molecules per m^2.

The chemical composition and surface coverage of UV-grafted PDMS layers were studied by angle-resolved XPS. In this case, silicone oil was grafted onto polished austenitic stainless steel substrates. The high-resolution XPS spectra are shown in Figure 1c−f. The XPS spectra of polished stainless steel consisted of Fe, Cr, Mo, O, and C peaks that were associated with an austenitic stainless steel alloy, native oxide film, and adventitious carbon (Figure S2, Supporting Information).[52] When UV grafted, the survey XPS spectra consist of Si, O, and C peaks associated with the PDMS, while the Fe 2p peak from the substrate is barely noticeable (Figure S2a, Supporting Information). The high-resolution XPS spectrum of Si 2p consists of a single peak at the binding energy of 102.4 eV (Figure 1c), which can be deconvoluted into two main components at 102.3 and 103.0 eV, corresponding to Si−C and Si−O bonds (Figure S3a, Supporting Information).[53] The high-resolution O 1s spectra (Figure 1d) reveal the main O 1s peak centered at 532.4 eV and a shoulder at 530.5 eV, which can be deconvoluted into three components (Figure S3b, Supporting Information), namely (i) the shoulder at 530.2 eV attributed to Me−O−Me bonds, where Me represents Fe, Ni, and Cr components of the substrate,[51] (ii) the main peak at 532.4 eV corresponding to the Si−O−Si bond,[54] and (iii) the peak at 533.1 eV to the O−Si−O bond (Figure S3b, Supporting Information).[55] Note that the shoulder at 530.2 eV is clearly observed at a measured angle of 75° (Figure 1d, red spectrum), but disappears when the angle is reduced to 15°, indicating complete coverage of the surface by the grafted PDMS molecules (Figure 1d, blue spectrum). The C 1s spectrum displays a single peak at 284.8 eV, which is associated with Si−C bonds in silicone oil (Figure 1e).[56] The high-resolution XPS Fe 2p signal is barely noticeable at a 75° angle and disappears completely when measured at a 15° angle (Figure 1f); the latter further corroborates that the PDMS grafted layer covers the substrate entirely. The Si and Fe XPS sputter profiles of UV-grafted PDMS are presented in Figure 1g. The thickness of the UV-grafted PDMS oil of 500 cSt viscosity, obtained by XPS measurements, was ∼9 nm (when the bulk polished stainless steel is reached), correlating well with ellipsometric measurements. However, the overlayer of unbound silicone oil is much thicker, varying as a function of oil viscosity. Here, we examined the overlayer thicknesses of silicon oil with viscosities starting from 2 to 1000 cSt using confocal microscopy; the results are presented in Figure 1h. As shown, the overlayer thickness increases from a single to tens of microns in this range of viscosities. This can be attributed to untangling and higher mobility of the grafted PDMS molecules in the presence of silicone oil due to complete miscibility and matching interfacial energies.[57] Furthermore, it is common knowledge that silicones tend to stick to surfaces,[58] and it is not an easy task to remove silicon oil even by its dissolution in a good solvent such as toluene.[38,59]

The corrosion of metals is a wetting-associated phenomenon that occurs due to the intimate contact of corrosive liquids with a solid substrate, affecting numerous industries, domestic applications, and public sectors worldwide. Effective corrosion inhibition has a high economic value as annual corrosion expenses are estimated to reach ∼4% of GDP in developed countries.[60] Austenitic grade stainless steels are commonly used as a construction and storage material due to their very good corrosion resistance, that is, tanks, storage vessels, and pipes in various fields and industries including electrical, construction, nuclear power, petrochemical, oil, gas, food processing, pharmaceutical, and transportation.[61] Marine applications are extremely demanding, while it is common knowledge by far that

https://doi.org/10.1021/acsami.2c04960
ACS Appl. Mater. Interfaces 2022, 14, 29386−29397

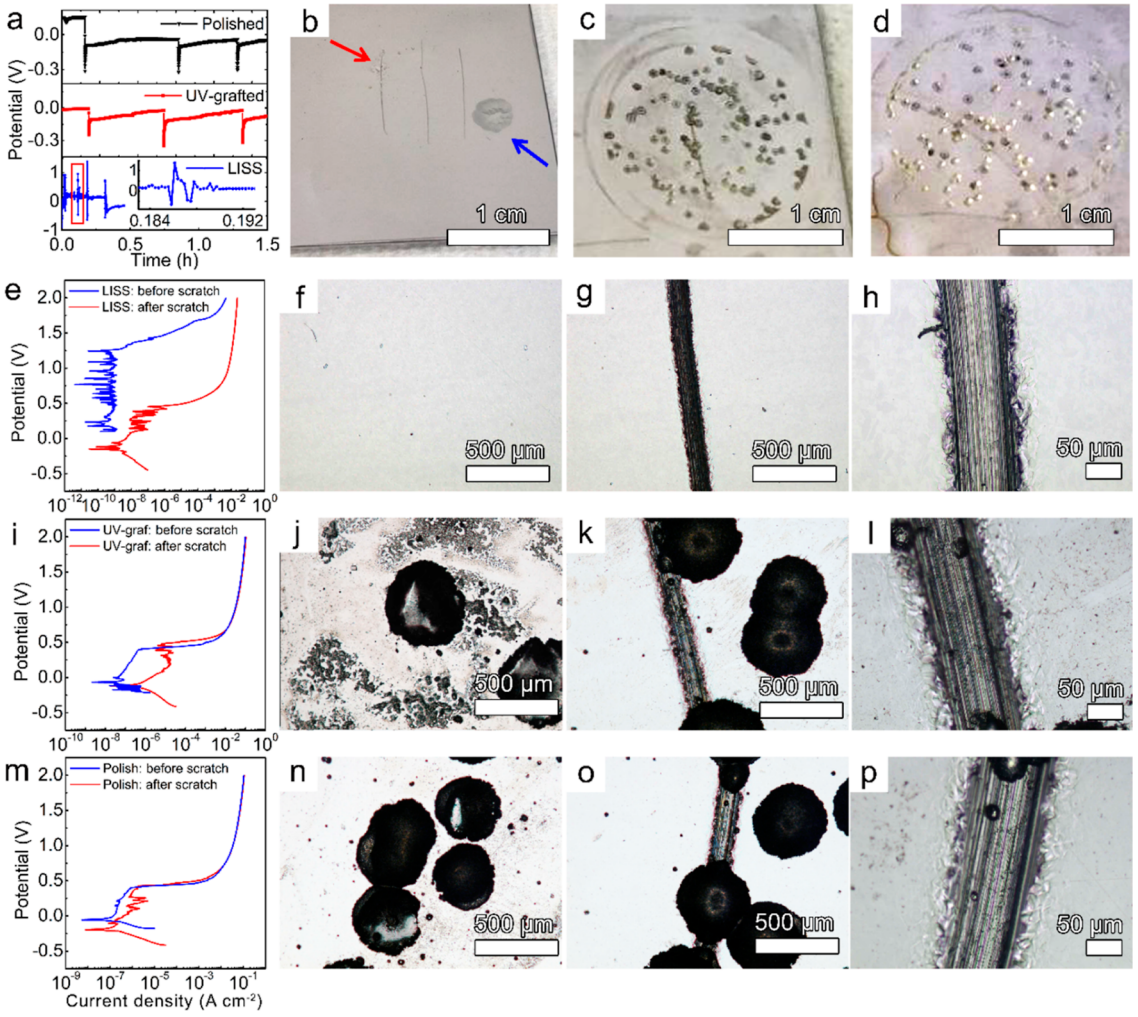

Figure 2. (a) OCP measurements as a function of time in 3.5 wt % NaCl aqueous solution of as-polished (top pattern, black line), UV-grafted (middle pattern, red line), and PDMS LISS (bottom pattern, blue line) measured during scratching. The inset in the bottom plot represents part of the chart inside the red frame. (b–d) Digital still images, (e,i,m) corresponding potentiodynamic polarization patterns, and (f–h,j–l,n–p) bright-field optical microscopy images (various magnifications) of PDMS LISS (b,e–h), PDMS UV-grafted (c,i–l), and as-polished bare (d,m–p) stainless steel samples after scratching and the potentiodynamic polarization measurements. (f,j,n) Images display area outside of the scratch, while (g,h,k,l,o,p) display the scratched area after the potentiodynamic polarization measurements.

stainless steels are susceptible to localized corrosion in seawater ranging from the AISI 300 series and up to superduplex grade steels.[62]

Because corrosion of metals in a marine environment is a vital problem, the hydrophobic coating may protect metallic substrates against corrosive media by minimizing their direct contact.[63] Previously, we demonstrated that LISS prepared on bare flat substrates can successfully delay corrosion of metals such as Al, Cu, and steel demonstrating so far the best anti-corrosion performance under neat conditions.[38] However, mechanical damage of surfaces occurs, commonly exposing unprotected areas, which can potentially initiate corrosion, finally leading to the failure of the protected area. Therefore, in this study, we examined the corrosion characteristics of PDMS-based LISS samples prepared on polished 316L grade stainless steel substrates while the surface was gradually damaged (Figure 2). The damage was produced by scratching the polished LISS substrates using a diamond scraper, forming torn rough-edge scratches of an average width of 50–100 μm and a typical depth of ca. 6 μm (Figure S4, Supporting Information).

Figure 2a shows a continued measurement of the OCP in the 3.5 wt % NaCl aqueous solution, while bare-polished, UV-grafted, and LISS substrates were damaged using a diamond scraper. The bare substrate shows an initial OCP value of 0.15 V that is reduced abruptly after scratching, that is, by exposing the plain metallic surface to the corrosive medium. Subsequently, the formation of a new passive oxide layer (repassivation process) leads to a progressive increase of OCP until reaching a stable value of −0.035 V. The same procedure was repeated several times, confirming the reproducibility of this tendency. The UV-grafted sample demonstrated a similar tendency to return to the original value of −0.025 V after each scratch, again due to the repassivation of the exposed plain metallic substrate with similar kinetics to the bare substrate. In contrast, the LISS samples presented in the case of the first two scratches an almost immediate return to the initial OCP 0.18 V value, produced by the self-healing capabilities of LISS surfaces by re-sealing the damaged area with faster kinetics than the repassivation of the scratched surface, that is, due to the presence of the lubricating liquid layer that is immiscible in corrosive medium (in this case, the aqueous NaCl solution) (see also Figure S5, Supporting

https://doi.org/10.1021/acsami.2c04960
ACS Appl. Mater. Interfaces 2022, 14, 29386–29397

Information).[20] Such a self-healing process can be envisioned by water droplets sliding on the bare and damaged LISS substrates tilted at ~60° (Movie S1, Supporting Information). As shown, droplets slide down identically on the undamaged LISS substrate and on the damaged LISS a few seconds after the scratching. However, in the case of the third scratch, the trend was similar to the bare and UV-grafted samples, indicating an insufficient recovery of the lubricant layer on this scratch. To confirm this hypothesis and identify regions of the scratches that were re-sealed and non-sealed, potentiodynamic polarizations were performed on the samples after concluding the scratches and OCP measurements. As shown in Figure 2m–p, the bare substrate shows typical characteristics of stainless steel AISI 316L in a chloride-containing electrolyte with an OCP value of −0.05 V and the onset for pitting corrosion at approximately 0.4 V. After the scratch, the OCP value is cathodically shifted to −0.2 V, the passive current increases, showing current peaks (transients), which are likely due to metastable pitting, while the pitting potential is maintained. Figure 2d shows that the surface is homogeneously covered by pits, both in the scratch and the rest of the surface, covering approx. 13% of the corroded area. The UV-grafted sample shows similar values to that obtained on the bare substrate with an OCP of −0.07 V and a pitting potential of 0.4 V, while after scratching the surface the OCP was reduced to −0.12 V, the onset of pitting corrosion was slightly increased to 0.48 V, and the passive current was significantly increased (Figure 2i). Here, the sample also displays pits in both the scratched and unscratched surfaces, displaying approx. 16% of the corroded area (Figure 2j–l). The highest difference occurs with the LISS sample, where the initial polarization curve demonstrates very low current densities prior to passivity breakdown at very high anodic potentials (pitting potential at 1.25 V) due to the low conductivity of the infused lubricating layer, which separates the corrosive medium from touching a metallic surface (Figure 2e). The noise in the i/E plot of the LISS sample stems from the low conductivity of the liquid-infused coating and, thus, very low anodic and cathodic currents through a wide range of potentials (Figure 2e, blue curve). After scratching, the part of the damaged area that was not re-sealed by the lubricant was exposed to the aggressive electrolyte concentrating corrosion under anodic polarization. As observed in Figure 2b and f–h, the scratches were mainly corrosion-free, except for the upper half of the left scratch (as indicated by a red arrow) and a localized region on the right side of the sample (as indicated by a blue arrow), possibly due to a defect in the coating, while both corroded pits represent ~ 3% of the overall area. The latter demonstrates again the importance of the self-healing characteristics of the LISS to improve corrosion resistance, while the defect sites, such as scratches of tens of micrometers, were resealed with the liquid lubricant, contributing to the enhanced corrosion protection, similarly to the SLIPS.[64]

Another phenomenon associated with the wetting of solid surfaces in marine environments is the formation of biofilms, commonly called "biofouling". Biofilms contain a diverse variety of micro-organisms. Within minutes of immersing a clean surface in water, it adsorbs organic materials named the "conditioning film". As a next step, bacteria colonize within hours, and unicellular algae and cyanobacteria (blue-green algae).[65] Fouling organisms that settle on and adhere to the immersed surfaces induce corrosion and drag, reducing the speed of ships, and simultaneously raising significantly their fuel consumption; therefore, the attachment of biofilms should be prevented. For the diversity, we used two freshwater green algae strains such as (i) *Chlorella sorokiniana* (*C. sorokiniana*)—a nonmotile thermotolerant unicellular algae with a high growth rate, being one of the most promising strains for industrial cultivation of microalgae;[66] and (ii) *Chlamydomonas reinhardtii* (*C. reinhardtii*)—a biflagellated motile unicellular algae that uses flagella as an effective tool for providing contact and cell adhesion to surfaces[67] as a model for aquatic organisms to explore the growth and adhesion of such algae biofilms on LISS and controlled substrates (Figure 3a). It should be noted,

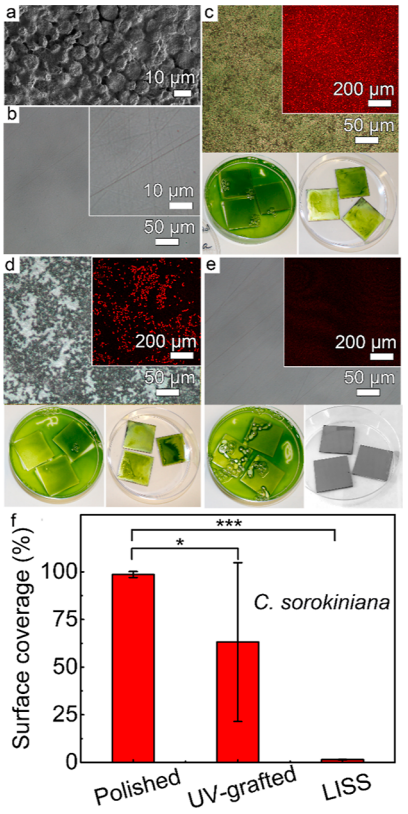

Figure 3. (a) SEM image of the freshwater green algae biofilm of type *C. sorokiniana*. Bright-field reflectance and confocal fluorescent (insets) images of polished 316L grade stainless steel substrates (b) before biofouling exposure and after 8 days of exposure to (c–e) freshwater green algae (*C. sorokiniana*). Austenitic stainless steel substrates of the following modifications were examined: (c) plain-polished, (d) polished PDMS UV-grafted, and (e) polished LISS. (f) Surface coverage area fraction calculated from fluorescent confocal microscopy images. Triplets were used for statistical analysis, and 10 independent images were measured for every sample.

however, that to the best of our knowledge, the relationship between individual cell adhesion and biofilm formation is still quite limited, whereas we and others have shown previously that such green algal biofilms, grown on treated surfaces, have proven to be remarkable indicators of the presence and effectiveness of a continuous, immobilized lubricant layer.[27,41,42] We, therefore, immersed the LISS and controls, that is, plain-polished and UV-grafted, stainless steel samples in freshwater growth media with green algae for 8 days under 16 h/8 h daylight/dark illumination cycles; the results are summarized in Figure 3b–f. Over the growth period, there was a notable increase in algae density with no sign of substrate-related growth reduction or mortality,

https://doi.org/10.1021/acsami.2c04960
ACS Appl. Mater. Interfaces 2022, 14, 29386–29397

indicating the nontoxic nature of the coating (Figure S6, Supporting Information).

As shown in Figure 3c–e, green freshwater algae of type *C. sorokiniana* grow uniformly in Petri dishes and on stainless steel samples. When the PDMS LISS samples were pulled through an air–water interface, 98.5 ± 0.4% of the attached biofilm was spontaneously delaminated, leaving behind clean, polished, and highly reflective steel surfaces (Figure 3e–f, and Movie S2, Supporting Information). The delamination of an interconnected, intact algae biofilm indicates its poor adhesion to the LISS-coated steel substrates, allowing passive easy shedding of the attached algae during air–water interface transition. In contrast, biofilms were firmly attached to both untreated and UV-grafted steel surfaces during the removal process, leaving behind 98.5 ± 1.5 and 63.1 ± 41.6% fouled surfaces, respectively (Figure 3c–d,f, and Movie S3, Supporting Information). Yet, there is a substantial difference in biofilm organization between bare and UV-grafted samples. Although green algae biofilms, grown on the bare polished steel samples, cover continuously the entire area (Figure 3c and Movie S3, Supporting Information), they show an uneven growth mode on the UV-grafted steel samples (Figure 3d and Movie S3, Supporting Information). The latter can be ascribed to weaker adhesion to the PDMS UV-grafted layer, as observed in several samples by biofilm sliding as soon as they pass through the air–water interface. This can be observed on the right sample in Figure 3d by the appearance of the intense green color. Statistical analysis was performed to determine the significance of the resistance of coated samples to aquatic biofouling, demonstrating a p-value of 0.028 and $\ll$0.005 for UV-grafted and LISS samples, respectively (Figure 3f).

To date, we have demonstrated that LISS substrates can prevent aquatic organism attachment. However, AF functions may readily be interfered with and finally lost due to detachment of the coating or damage commonly occurring through operation in water.[68] Although the problem of detached fragments of loosely bound porous coating, as required for SLIPS, was solved by infusing the lubricating liquid on a bare flat substrate, mechanical scratches still normally occur during the operation. Therefore, it is important to examine how robust the anti-biofouling characteristics of LISS substrates are. Here, we applied gradual scratching of LISS and control, that is, as-polished and UV-grafted substrates just before their exposure to the aquatic organisms' environment. In addition, the stainless steel SLIPS samples were also examined and compared to their LISS counterparts. Defects were produced by damaging the polished steel surfaces using a diamond scraper. Two, four, and six lines were scratched over the entire sample width and length (Figure S7, and Movie S4, Supporting Information). Immediately after the scratching, all the samples were immersed in a Petri dish with freshwater green algae of type *C. reinhardtii* for an 8 day incubation period. Here, the adhesion strength of both green algae strains is of the same order of magnitude,[67,69] while *C. reinhardtii* is a biflagellated algae strain, that is, motile algal cells, can migrate in the aquatic environment searching for nutrients and optimal light exposure but also the damaged but non-self-healed areas serving as adhesion points for algal attachment.

As previously shown, green algae biofilms grow uniformly in a Petri dish and on stainless steel samples (Figure 4a–d), while a noticeable increase in color intensity was observed for control and LISS/SLIPS samples (Figure S8, Supporting Information). When the PDMS LISS samples were pulled through an air–water interface, 73.5 ± 10.6% of the attached biofilm was spontaneously delaminated leaving behind a clean, polished steel surface and scratched areas (Figure 4c, middle image, h-panel, k, and Movie S5, Supporting Information). The latter emphasizes the self-healing characteristics of LISS substrates in which the infused mobile lubricant re-seals the damaged area, protecting it from the organism attaching. Such delamination of the algae biofilm indicates again its poor adhesion to the LISS-coated underlying steel substrates, allowing easy shedding during the air–water interface pulling. However, as shown in Figure 4c, middle image, the algae biofilm ruptured at scratches, which can be attributed mainly to the torn rough scratched edges. It should be noted that individual algae were observed within the scratched area, mainly near the intersection of two scratches (Figure S9, Supporting Information). The latter may be attributed to the fact that the self-healing kinetics (and particularly underwater) may take a longer time than that

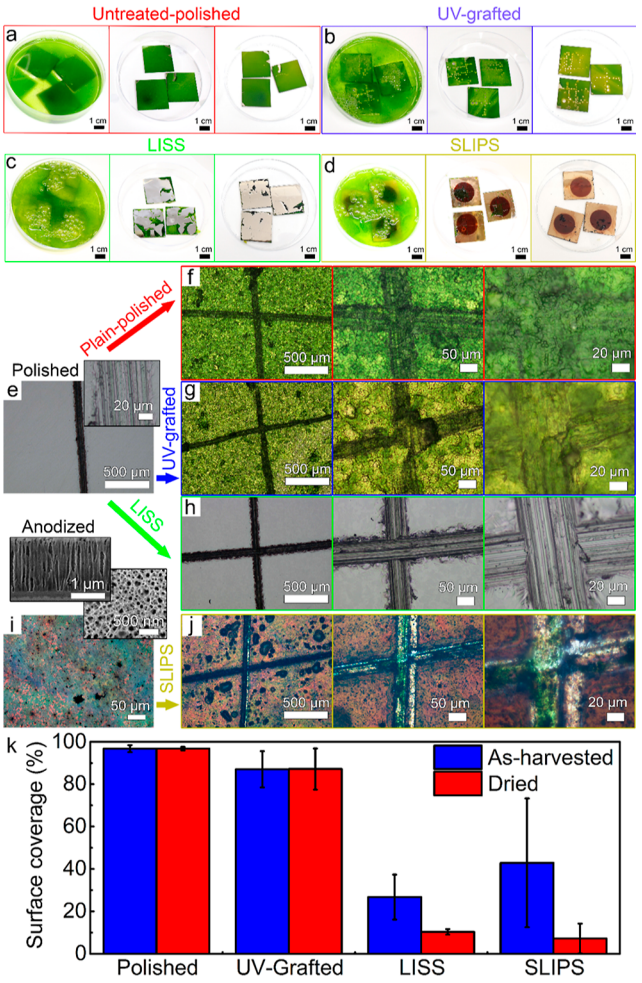

Figure 4. (a–d) Digital images of the samples before (left image), just after the harvesting (middle image), and after drying at an ambient atmosphere (right image). (f–j) Bright-field reflectance microscopy images of the samples after damage with a diamond scraper (e), and after exposure for 8 days to (f–j) freshwater motile green algae of type *C. reinhardtii*. Austenitic 316L stainless steel substrates of the following modifications were examined: (f) as-polished, (g) polished PDMS UV-grafted, (h) polished PDMS LISS, and (j) anodized PDMS SLIPS. Insets in (i) are top-view and cross-sectional high-resolution SEM images of as-anodized 316L stainless steel substrates. (k) Calculated surface coverage area fraction of just-harvested and dried samples. Triplets were used in all the experiments for statistical analysis.

https://doi.org/10.1021/acsami.2c04960
ACS Appl. Mater. Interfaces 2022, 14, 29386–29397

required for a motile individual alga to settle on a heavily damaged (intersection) unprotected surface. Yet, the appearance of individual alga cells may indicate that the self-healing process occurs underwater as well, further preventing the development of a biofilm. In contrast, biofilms attached firmly to both polished and UV-grafted steel substrates during the removal process, leaving 96.8 ± 1.7 and 87.1 ± 8.6% fouled surfaces, respectively (Figure 4a,b,k). It should be noticed that the green color intensity was more pronounced on the plain-polished samples compared to the UV-grafted ones, that is, due to higher reflectance, indicating that the thickness of biofilm grown on the UV-grafted samples is thinner (Figure 4a,b, right images). Furthermore, the formation of stable bubbles on the UV-grafted samples was also observed near the scratches, leaving behind almost biofouling-free areas (Figure 4b, the right image, and Figure S10, Supporting Information).

Finally, for the comparison of the biofouling characteristics of LISS substrates, we used state-of-the-art SLIPS,[70] prepared by electrochemical anodization of stainless steel samples to form a porous oxide layer followed by UV-grafting of PDMS (Figure 4i, inset images).[44] Here, the μm thick porous oxide layer was obtained with nanometer-scale porosity. We and others demonstrated excellent repellent characteristics of SLIPS substrates prepared by various techniques; however, these characteristics were mainly obtained on plain, undamaged SLIPS substrates.[21,22,27,28,37,38,70−72] Here, SLIPS substrates were damaged similarly to LISS substrates and then examined for their anti-biofouling characteristics; the results are summarized in Figure 4d,j,k. As shown, the damaged SLIPS substrates demonstrate an intact morphology, that is, there was no detachment or delamination of the oxide porous layer, while only a smashed area indicates that the oxide layer adheres well to the underlying metallic substrate. The as-harvested SLIPS samples demonstrated 42.9 ± 30.4% fouled surface coverage, while the biofilms ruptured during the pulling through an air−water interface mainly at the scratches, that is, on the torn rough scratch edges (Figure 4d, and Movie S5, Supporting Information).

The as-harvested samples were dried at an ambient atmosphere. As shown in Figure 4a−d,k, right images, the biofilm retracts further on LISS and SLIPS samples. Such retraction of algae biofilms on slippery surfaces upon drying may be attributed to the dehydration of green algae, leading primarily to a shrinkage process of the intact biofilm.[73] The dehydration process occurs in all the samples, while in the case of LISS/SLIPS, such stresses overwhelm the weak adhesion of the biofilms, causing their shrinkage. Furthermore, such retraction performance may be an indicator of the broadscale FR performance of the anti-biofouling coatings.[74,75] The fouled surface coverage on the dried samples decreased to 10.3 ± 1.3 and 7.2 ± 6.9% of the total area for LISS and SLIPS substrates, respectively, indicating comparable biofouling repellent characteristics (Figure 4k). It should be noted that the non-anodized area of the SLIPS samples, that is, the area outside of the brown circle, was also completely clean from the biofilm. This indicates that the area outside of the brown circle is the LISS one, differing from the regularly prepared LISS samples only by the annealing in air at 450 °C for 1 h before the UV-grafting process. In contrast, no further retraction of the algae biofilm was observed in both the plain-polished and UV-grafted substrates (Figure 4a,b, right images). These results demonstrate that LISS substrates compete well with the state-of-the-art SLIPS substrates while the preparation processes of LISS are facile and their mechanical durability is similar to the substrate bulk material.

Although bacteria are usually associated with primary biofilm communities, other microscopic organisms such as diatoms are also known as early colonizers.[40,43] Diatoms are the world's most diverse group of algae, comprising more than 10^5 species.[76] Diatoms are unicellular algae in which the protoplast is enclosed in an elaborately ornamented silica case (the frustule) composed of overlapping halves or "valves" (Figure 5a).[77] Diatoms adhere

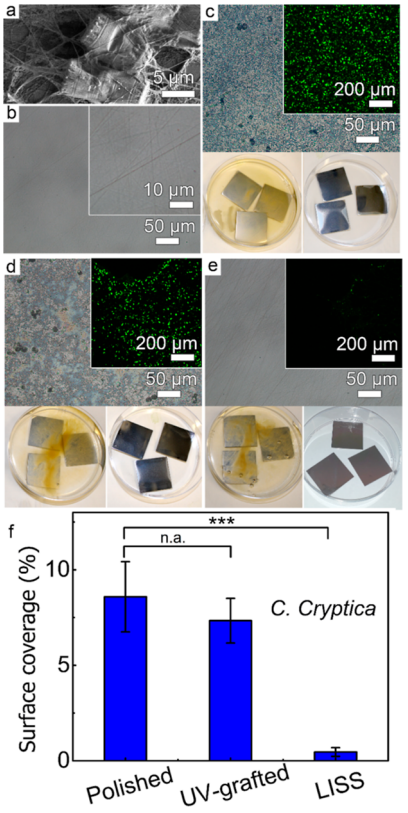

Figure 5. (a) SEM image of seawater diatom biofilms of type *C. cryptica*. Bright-field reflectance and confocal fluorescent (insets) images of polished 316L grade stainless steel substrates (b) before biofouling exposure and after 8 days of exposure to (c−e) seawater diatoms (*C. cryptica*). Austenitic stainless steel substrates of the following modifications were examined: (c) plain-polished, (d) polished PDMS UV-grafted, and (e) polished LISS. (f) Surface coverage area fraction calculated from fluorescent confocal microscope images. Triplets were used for statistical analysis, and 10 independent images were measured for every sample.

to surfaces through the production of sticky extracellular polymeric substances (Figure 5a), which are secreted through an elongate slit in one or both valves, while the division of attached cells rapidly gives rise to colonies, which eventually coalesce to form a compact biofilm.[78]

The demand for nontoxic AF coatings has led to an increased interest in silicone elastomers, which "release" fouling organisms under hydrodynamic conditions. Previous experiments on PDMS elastomers demonstrated that diatoms can hardly be released even at high-speed operating conditions (>30 knots).[40,78] Hence, it is vital to examine the developed LISS coating on its FR properties versus early colonizers such as seawater diatoms of the type *Cyclotella cryptica* (*C. cryptica*) (Figure 5a).[79] Within 8 days of immersion, growth of diatoms in

https://doi.org/10.1021/acsami.2c04960
ACS Appl. Mater. Interfaces 2022, 14, 29386−29397

LISS and control samples was observed (Figure 5c−e, still images). It should be noted that surface coverage of the diatom biofilm calculations is challenging using digital and reflectance microscopy images due to low color contrast (Figure 5c−e, still digital, optical microscope images, and Movie S6, Supporting Information). Here, the calculations were performed using confocal fluorescence microscopy images, in which surface coverage was obtained by means of the average fluorescent signal (Figure 5c−e, inset images). Both plain-polished and UV-grafted samples were pulled through an air−water interface, demonstrating surface coverage of 8.6 ± 1.8 and 7.3 ± 1.2%, respectively (Figure 5c,d,f). At the same time, the surface coverage of the LISS samples was 0.4 ± 0.2%, indicating a significant difference ($p \ll 0.005$) compared to bare and UV-grafted samples (Figure 5e,f). Again, passive shedding, that is, no external energy/stimuli were applied to remove the biofilm from the surface while the sample was pulled through an air−water interface, points out poor adhesion of the diatom biofilms to the LISS-coated steel substrates.

CONCLUSIONS

In this study, we further explored a one-pot approach of UV-grafting of PDMS to adopt the surface of virtually any solid material to liquid-infused slippery substrates (LISS). To form LISS substrates, PDMS was covalently grafted to a substrate by UV light of a specific wavelength, while PDMS serves as a reducing surface energy agent and infuses lubricants simultaneously. The proposed approach is simple to implement, rapid, nontoxic, environmentally friendly, easily scalable, and low-cost, yet forms a stable liquid-infused slippery coating. Furthermore, no pre-/post-grafting treatments, or harsh treatment conditions, and micro- or hierarchical micro-/nanosurface structuring are required to form LISS for industrial applications, making it advantageous over superhydrophobic and SLIPS surfaces; that is, the LISS substrates are as mechanically robust as the bare bulk material. Previously, we demonstrated that LISSs display enhanced corrosion resistance, reduced friction, and excellent repellency to complex fluids such as blood and both Gram-positive and Gram-negative bacteria biofilm adhesion. Here, we extended the study by gradually damaging LISS and control substrates by scratching the surface, creating microscale grooves that mimic damage that commonly occurs under operating conditions. We showed that the self-healing properties of the liquid-infused lubricating layer allow effective resealing of such microscale grooves, protecting the metallic surface from direct contact with the corrosive medium.

Because of the nontoxicity of silicone-based compounds, a UV-grafted process was applied on marine-applicable stainless steel substrates. We demonstrate that LISS substrates can successfully prevent the adhesion of aquatic organisms such as freshwater green algae and seawater diatoms after 8 days of exposure in laboratory conditions. Furthermore, we examined the influence of mechanical damage of LISS and controlled surfaces on the adhesion of biofilms. For that, the polished steel surface was damaged gradually by microscopic size scratches, and thereafter immersed for 8 days in aquatic culture. The damaged LISS surfaces were then compared to state-of-the-art SLIPS surfaces, which were damaged in the same way. Comparable results were obtained on both types of slippery surfaces, while from the technological point of view, the formation of LISS samples is much simpler. This is due to the fact that the formation of SLIPS substrates requires a three-step procedure (i.e., structuring of the substrate surface to form a porous coating, surface functionalization to reduce the surface energy of the developed porous coating, and finally lubrication), while the formation of LISS substrates consists only of a single step, that is, lubrication of the surface by silicon oil utilized for surface modification (UV grafting) with the remnant oil used for lubrication. It should be noted, however, that the underwater anti-biofouling performance of our LISS coating was examined during short-term laboratory conditions, while to compare it to SLIPS technology,[80] the long-term experiments, that is, field studies, should be performed in various geographical places under different temperatures and salinity conditions. Given all the aforementioned advances, and considering that our LISSs can be applied to various materials such as metals, metal oxides, ceramics, glasses, and so forth, we envision that our UV-grafting approach of the PDMS-based LISS will push forward the development of nontoxic repellent coating technology toward challenging and extremely desirable marine anti-biofouling applications.

ASSOCIATED CONTENT

Supporting Information

The Supporting Information is available free of charge at https://pubs.acs.org/doi/10.1021/acsami.2c04960.

Typical UV−visible spectrum of a medium-pressure mercury UV lamp, XPS spectra of bare and UV-grafted polished stainless steel substrates, measured and deconvoluted XPS Si 2p and O 1s spectrum of 500 cSt PDMS oil UV grafted to stainless steel, optical microscopy and atomic force microscopy images of the as-polished 316L grade stainless steel after scratching, OCP measurements during and immediately after substrate damage of the LISS sample, digital images of green algae and diatom assays before and after 8 days of growing in Petri dishes with samples, digital images of the scratched polished stainless steel samples, digital images of as-immersed and after 8 days of immersion into freshwater green algae,) optical microscopy images of scratches with green algae attached, and optical microscopy images of the UV-grafted sample under the bubble area after 8 days of immersion in green algae (PDF)

Self-healing characteristics of the LISS prepared on stainless steel substrates (MP4)

Green algae biofilm shading from an undamaged LISS surface during transition through a water−air interface (MP4)

Green algae biofilm shading from undamaged bare and UV-grafted surfaces during transition through a water−air interface (MP4)

Scratching of LISS surfaces before exposure to algae biofouling (MP4)

Green algae biofilm shading from damaged bare, UV-grafted, and LISS surfaces during transition through a water−air interface (MP4)

Diatom biofilm shading from undamaged bare, UV-grafted, and LISS surface during transition through a water−air interface (MP4)

AUTHOR INFORMATION

Corresponding Authors

Alexander B. Tesler − *Faculty of Engineering, Department of Materials Science and Engineering, Institute for Surface Science*

https://doi.org/10.1021/acsami.2c04960
ACS Appl. Mater. Interfaces 2022, 14, 29386−29397

and Corrosion, Friedrich-Alexander-Universität Erlangen-Nürnberg, Erlangen 91058, Germany; orcid.org/0000-0003-3425-7667; Email: alexander.tesler@fau.de

Wolfgang H. Goldmann − *Department of Physics, Biophysics Group, Friedrich-Alexander-Universität Erlangen-Nürnberg, Erlangen 91052, Germany*; Email: wolfgang.goldmann@fau.de

Authors

Lucia H. Prado − *Faculty of Engineering, Department of Materials Science and Engineering, Institute for Surface Science and Corrosion, Friedrich-Alexander-Universität Erlangen-Nürnberg, Erlangen 91058, Germany*

Ingo Thievessen − *Department of Physics, Biophysics Group, Friedrich-Alexander-Universität Erlangen-Nürnberg, Erlangen 91052, Germany*

Anca Mazare − *Faculty of Engineering, Department of Materials Science and Engineering, Institute for Surface Science and Corrosion, Friedrich-Alexander-Universität Erlangen-Nürnberg, Erlangen 91058, Germany*

Patrik Schmuki − *Faculty of Engineering, Department of Materials Science and Engineering, Institute for Surface Science and Corrosion, Friedrich-Alexander-Universität Erlangen-Nürnberg, Erlangen 91058, Germany; Chemistry Department, Faculty of Sciences, King Abdul-Aziz University, Jeddah 80203, Saudi Arabia; Regional Centre of Advanced Technologies and Materials, Palacky University, Olomouc 772 07, Czech Republic;* orcid.org/0000-0002-9208-5771

Sannakaisa Virtanen − *Faculty of Engineering, Department of Materials Science and Engineering, Institute for Surface Science and Corrosion, Friedrich-Alexander-Universität Erlangen-Nürnberg, Erlangen 91058, Germany*

Complete contact information is available at: https://pubs.acs.org/10.1021/acsami.2c04960

Author Contributions

A.B.T. and L.H.P. contributed equally. The manuscript was written with contributions from all the authors. All the authors have approved the final version of the manuscript.

Notes

The authors declare no competing financial interest.

■ ACKNOWLEDGMENTS

The authors acknowledge the DFG and DFG Cluster of Excellence EAM for financial support. A.B.T. and W.H.G. would like to acknowledge the DFG (grant number 442826449; SCHM 1597/38-1 and FA 336/13-1) for financial support. We thank Nuremberg Zoo for providing us with the recipe to prepare seawater for the seawater organism medium. We thank Mr. Johannes Harrer and Prof. Nicolas Vogel for their support with atomic force microscopy measurements. We thank Ms. Helga Hildebrand for the XPS measurements and Ms. Vanessa Goetz for helping with the ellipsometric measurements. We thank Mr. Stefan Kölle for the fruitful discussion of the biofouling experiments and results.

■ REFERENCES

(1) Zobell, C. E.; Allen, E. C. The Significance of Marine Bacteria in the Fouling of Submerged Surfaces. *J. Bacteriol.* **1935**, *29*, 239−251.

(2) Bazaka, K.; Jacob, M. V.; Crawford, R. J.; Ivanova, E. P. Efficient Surface Modification of Biomaterial to Prevent Biofilm Formation and the Attachment of Microorganisms. *Appl. Microbiol. Biotechnol.* **2012**, *95*, 299−311.

(3) Schultz, M. P.; Bendick, J. A.; Holm, E. R.; Hertel, W. M. Economic Impact of Biofouling on a Naval Surface Ship. *Biofouling* **2011**, *27*, 87.

(4) Bannister, J.; Sievers, M.; Bush, F.; Bloecher, N. Biofouling in Marine Aquaculture: A Review of Recent Research and Developments. *Biofouling* **2019**, *35*, 631−648.

(5) Railkin, A. I. *Marine Biofouling: Colonization Processes and Defenses*; CRC Press INC.: Boca Raton, 2003; p 320.

(6) Whalan, S.; Webster, N. S. Sponge Larval Settlement Cues: The Role of Microbial Biofilms in a Warming Ocean. *Sci. Rep.* **2014**, *4*, 4072.

(7) Woods Hole Oceanographic Institution. Chapter 11: The History of the Prevention of Fouling. *Marine Fouling and Its Prevention; Prepared for Bureau of Ships, Navy Department*; George Banta Publishing Company: Menasha, Wisconsin, 1952; p 388.

(8) Lejars, M.; Margaillan, A.; Bressy, C. Fouling Release Coatings: A Nontoxic Alternative to Biocidal Antifouling Coatings. *Chem. Rev.* **2012**, *112*, 4347−4390.

(9) Banerjee, I.; Pangule, R. C.; Kane, R. S. Antifouling Coatings: Recent Developments in the Design of Surfaces That Prevent Fouling by Proteins, Bacteria, and Marine Organisms. *Adv. Mater.* **2011**, *23*, 690−718.

(10) Han, X.; Wu, J.; Zhang, X.; Shi, J.; Wei, J.; Yang, Y.; Wu, B.; Feng, Y. Special Issue on Advanced Corrosion-Resistance Materials and Emerging Applications. The Progress on Antifouling Organic Coating: From Biocide to Biomimetic Surface. *J. Mater. Sci. Technol.* **2021**, *61*, 46−62.

(11) Schumacher, J. F.; Carman, M. L.; Estes, T. G.; Feinberg, A. W.; Wilson, L. H.; Callow, M. E.; Callow, J. A.; Finlay, J. A.; Brennan, A. B. Engineered Antifouling Microtopographies - Effect of Feature Size, Geometry, and Roughness on Settlement of Zoospores of the Green Alga Ulva. *Biofouling* **2007**, *23*, 55.

(12) Bers, A. V.; Wahl, M. The Influence of Natural Surface Microtopographies on Fouling. *Biofouling* **2004**, *20*, 43.

(13) Sokolova, A.; Cilz, N.; Daniels, J.; Stafslien, S. J.; Brewer, L. H.; Wendt, D. E.; Bright, F. V.; Detty, M. R. A Comparison of the Antifouling/Foul-Release Characteristics of Non-Biocidal Xerogel and Commercial Coatings toward Micro- and Macrofouling Organisms. *Biofouling* **2012**, *28*, 511−523.

(14) Galhenage, T. P.; Hoffman, D.; Silbert, S. D.; Stafslien, S. J.; Daniels, J.; Miljkovic, T.; Finlay, J. A.; Franco, S. C.; Clare, A. S.; Nedved, B. T.; Hadfield, M. G.; Wendt, D. E.; Waltz, G.; Brewer, L.; Teo, S. L. M.; Lim, C.-S.; Webster, D. C. Fouling-Release Performance of Silicone Oil-Modified Siloxane-Polyurethane Coatings. *ACS Appl. Mater. Interfaces* **2016**, *8*, 29025−29036.

(15) Hwang, G. B.; Page, K.; Patir, A.; Nair, S. P.; Allan, E.; Parkin, I. P. The Anti-Biofouling Properties of Superhydrophobic Surfaces Are Short-Lived. *ACS Nano* **2018**, *12*, 6050−6058.

(16) Jokinen, V.; Kankuri, E.; Hoshian, S.; Franssila, S.; Ras, R. H. A. Superhydrophobic Blood-Repellent Surfaces. *Adv. Mater.* **2018**, *30*, 1705104.

(17) Lafuma, A.; Quéré, D. Superhydrophobic States. *Nat. Mater.* **2003**, *2*, 457−460.

(18) Poetes, R.; Holtzmann, K.; Franze, K.; Steiner, U. Metastable Underwater Superhydrophobicity. *Phys. Rev. Lett.* **2010**, *105*, 166104.

(19) Wang, D.; Sun, Q.; Hokkanen, M. J.; Zhang, C.; Lin, F.-Y.; Liu, Q.; Zhu, S.-P.; Zhou, T.; Chang, Q.; He, B.; Zhou, Q.; Chen, L.; Wang, Z.; Ras, R. H. A.; Deng, X. Design of Robust Superhydrophobic Surfaces. *Nature* **2020**, *582*, 55−59.

(20) Wong, T.-S.; Kang, S. H.; Tang, S. K. Y.; Smythe, E. J.; Hatton, B. D.; Grinthal, A.; Aizenberg, J. Bioinspired Self-Repairing Slippery Surfaces with Pressure-Stable Omniphobicity. *Nature* **2011**, *477*, 443−447.

(21) Amini, S.; Kolle, S.; Petrone, L.; Ahanotu, O.; Sunny, S.; Sutanto, C. N.; Hoon, S.; Cohen, L.; Weaver, J. C.; Aizenberg, J.; Vogel, N.; Miserez, A. Preventing Mussel Adhesion Using Lubricant-Infused Materials. *Science* **2017**, *357*, 668−673.

(22) Epstein, A. K.; Wong, T.-S.; Belisle, R. A.; Boggs, E. M.; Aizenberg, J. Liquid-Infused Structured Surfaces with Exceptional Anti-

Biofouling Performance. *Proc. Natl. Acad. Sci. U.S.A.* **2012**, *109*, 13182−13187.
(23) Howell, C.; Grinthal, A.; Sunny, S.; Aizenberg, M.; Aizenberg, J. Designing Liquid-Infused Surfaces for Medical Applications: A Review. *Adv. Mater.* **2018**, *30*, 1802724.
(24) Kim, P.; Wong, T.-S.; Alvarenga, J.; Kreder, M. J.; Adorno-Martinez, W. E.; Aizenberg, J. Liquid-Infused Nanostructured Surfaces with Extreme Anti-Ice and Anti-Frost Performance. *ACS Nano* **2012**, *6*, 6569−6577.
(25) Leslie, D. C.; Waterhouse, A.; Berthet, J. B.; Valentin, T. M.; Watters, A. L.; Jain, A.; Kim, P.; Hatton, B. D.; Nedder, A.; Donovan, K.; Super, E. H.; Howell, C.; Johnson, C. P.; Vu, T. L.; Bolgen, D. E.; Rifai, S.; Hansen, A. R.; Aizenberg, M.; Super, M.; Aizenberg, J.; Ingber, D. E. A Bioinspired Omniphobic Surface Coating on Medical Devices Prevents Thrombosis and Biofouling. *Nat. Biotechnol.* **2014**, *32*, 1134−1140.
(26) Li, J.; Kleintschek, T.; Rieder, A.; Cheng, Y.; Baumbach, T.; Obst, U.; Schwartz, T.; Levkin, P. A. Hydrophobic Liquid-Infused Porous Polymer Surfaces for Antibacterial Applications. *ACS Appl. Mater. Interfaces* **2013**, *5*, 6704−6711.
(27) Tesler, A. B.; Kim, P.; Kolle, S.; Howell, C.; Ahanotu, O.; Aizenberg, J. Extremely Durable Biofouling-Resistant Metallic Surfaces Based on Electrodeposited Nanoporous Tungstite Films on Steel. *Nat. Commun.* **2015**, *6*, 8649.
(28) Tesler, A. B.; Sheng, Z.; Lv, W.; Fan, Y.; Fricke, D.; Park, K.-C.; Alvarenga, J.; Aizenberg, J.; Hou, X. Metallic Liquid Gating Membranes. *ACS Nano* **2020**, *14*, 2465−2474.
(29) Vogel, N.; Belisle, R. A.; Hatton, B.; Wong, T.-S.; Aizenberg, J. Transparency and Damage Tolerance of Patternable Omniphobic Lubricated Surfaces Based on Inverse Colloidal Monolayers. *Nat. Commun.* **2013**, *4*, 2176.
(30) Hou, X.; Li, J.; Tesler, A. B.; Yao, Y.; Wang, M.; Min, L.; Sheng, Z.; Aizenberg, J. Dynamic Air/Liquid Pockets for Guiding Microscale Flow. *Nat. Commun.* **2018**, *9*, 733.
(31) Hou, X. Liquid Gating Membrane. *Natl. Sci. Rev.* **2019**, *7*, 9−11.
(32) Sheng, Z.; Zhang, J.; Liu, J.; Zhang, Y.; Chen, X.; Hou, X. Liquid-Based Porous Membranes. *Chem. Soc. Rev.* **2020**, *49*, 7907−7928.
(33) Zhang, J.; Chen, B.; Chen, X.; Hou, X. Liquid-Based Adaptive Structural Materials. *Adv. Mater.* **2021**, *33*, 2005664.
(34) Hou, X. Smart Gating Multi-Scale Pore/Channel-Based Membranes. *Adv. Mater.* **2016**, *28*, 7049−7064.
(35) Villegas, M.; Zhang, Y.; Abu Jarad, N.; Soleymani, L.; Didar, T. F. Liquid-Infused Surfaces: A Review of Theory, Design, and Applications. *ACS Nano* **2019**, *13*, 8517−8536.
(36) Chen, B.; Zhang, R.; Hou, Y.; Zhang, J.; Chen, S.; Han, Y.; Chen, X.; Hou, X. Light-Responsive and Corrosion-Resistant Gas Valve with Non-Thermal Effective Liquid-Gating Positional Flow Control. *Light: Sci. Appl.* **2021**, *10*, 127.
(37) Deng, R.; Shen, T.; Chen, H.; Lu, J.; Yang, H.-C.; Li, W. Slippery Liquid-Infused Porous Surfaces (SLIPSs): A Perfect Solution to Both Marine Fouling and Corrosion? *J. Mater. Chem. A* **2020**, *8*, 7536−7547.
(38) Tesler, A. B.; Prado, L. H.; Khusniyarov, M. M.; Thievessen, I.; Mazare, A.; Fischer, L.; Virtanen, S.; Goldmann, W. H.; Schmuki, P. A One-Pot Universal Approach to Fabricate Lubricant-Infused Slippery Surfaces on Solid Substrates. *Adv. Funct. Mater.* **2021**, *31*, 2101090.
(39) Vondráček, P.; Doležel, B. Biostability of Medical Elastomers: A Review. *Biomaterials* **1984**, *5*, 209−214.
(40) Hu, P.; Xie, Q.; Ma, C.; Zhang, G. Silicone-Based Fouling-Release Coatings for Marine Antifouling. *Langmuir* **2020**, *36*, 2170−2183.
(41) Howell, C.; Vu, T. L.; Lin, J. J.; Kolle, S.; Juthani, N.; Watson, E.; Weaver, J. C.; Alvarenga, J.; Aizenberg, J. Self-Replenishing Vascularized Fouling-Release Surfaces. *ACS Appl. Mater. Interfaces* **2014**, *6*, 13299−13307.
(42) Paink, G. K.; Kolle, S.; Le, D.; Weaver, J. C.; Alvarenga, J.; Ahanotu, O.; Aizenberg, J.; Kim, P. Dynamic Self-Repairing Hybrid Liquid-in-Solid Protective Barrier for Cementitious Materials. *ACS Appl. Mater. Interfaces* **2020**, *12*, 31922−31932.
(43) Robinson, N. J.; Majewska, R.; Lazo-Wasem, E. A.; Nel, R.; Paladino, F. V.; Rojas, L.; Zardus, J. D.; Pinou, T. Epibiotic Diatoms Are Universally Present on All Sea Turtle Species. *PLoS One* **2016**, *11*, No. e0157011.
(44) Prado, L. H.; Anastasiou, E.; Virtanen, S. Corrosion Behavior of a Slippery Liquid Infused Porous Surface on Anodized Stainless Steel. *Mater. Lett.* **2021**, *296*, 129892.
(45) Prado, L. H.; Anastasiou, E.; Virtanen, S. Corrosion Behavior of Anodic Self-Ordered Porous Oxide Layers on Stainless Steel. *J. Electrochem. Soc.* **2021**, *168*, 021507.
(46) Baensch, H. A.; Debelius, H. *Meerwasser Atlas*; Mergus, Verlag für Natur-und Heimtierkunde Baensch, 1992.
(47) Colter Stewart, J.; Shelley, M. N.; Schwartz, N. R.; King, S. K.; Boyce, D. W.; Erikson, J. W.; Allred, D. D.; Colton, J. S. Optical Constants of Evaporated Amorphous Zinc Arsenide (Zn_3As_2) Via Spectroscopic Ellipsometry. *Opt. Mater. Express* **2019**, *9*, 4677−4687.
(48) Acuna, N.; Rosado, C.; Valdez, B.; Schorr, M.; Hernandez-Duque, G. Effect of Marine Biofilin on Fatigue Resistance of an Austenitic Stainless Steel. *Corros. Rev.* **2004**, *22*, 101−114.
(49) Panagopoulos, A.; Loizidou, M.; Haralambous, K.-J. Stainless Steel in Thermal Desalination and Brine Treatment: Current Status and Prospects. *Met. Mater. Int.* **2020**, *26*, 1463−1482.
(50) Moller, G. E. The Successful Use of Austenitic Stainless Steels in Sea Water. *J. Soc. Pet. Eng.* **1977**, *17*, 101−110.
(51) Wooh, S.; Encinas, N.; Vollmer, D.; Butt, H.-J. Stable Hydrophobic Metal-Oxide Photocatalysts Via Grafting Polydimethylsiloxane Brush. *Adv. Mater.* **2017**, *29*, 1604637.
(52) Tardio, S.; Abel, M.-L.; Carr, R. H.; Castle, J. E.; Watts, J. F. Comparative Study of the Native Oxide on 316l Stainless Steel by XPS and Tof-Sims. *J. Vac. Sci. Technol., A* **2015**, *33*, 05E122.
(53) Kaur, A.; Chahal, P.; Hogan, T. Selective Fabrication of Sic/Si Diodes by Excimer Laser under Ambient Conditions. *IEEE Electron Device Lett.* **2016**, *37*, 142−145.
(54) Pertsin, A. J.; Gorelova, M. M.; Levin, V. Y.; Makarova, L. I. An Xps Study of the Surface−Bulk Compositional Differences in Siloxane-Containing Block Copolymers and Polymer Blends. *J. Appl. Polym. Sci.* **1992**, *45*, 1195−1202.
(55) Allen, G. C.; Curtis, M. T.; Hooper, A. J.; Tucker, P. M. X-Ray Photoelectron Spectroscopy of Iron−Oxygen Systems. *J. Chem. Soc., Dalton Trans.* **1974**, *14*, 1525−1530.
(56) Sabata, A.; van Ooij, W. J.; Yasuda, H. K. Plasma-Polymerized Films of Trimethylsilane Deposited on Cold-Rolled Steel Substrates. Part 1. Characterization by XPS, AES and Tof-Sims. *Surf. Interface Anal.* **1993**, *20*, 845−859.
(57) Wooh, S.; Vollmer, D. Silicone Brushes: Omniphobic Surfaces with Low Sliding Angles. *Angew. Chem., Int. Ed.* **2016**, *55*, 6822−6824.
(58) Teisala, H.; Baumli, P.; Weber, S. A. L.; Vollmer, D.; Butt, H.-J. Grafting Silicone at Room Temperature—a Transparent, Scratch-Resistant Nonstick Molecular Coating. *Langmuir* **2020**, *36*, 4416−4431.
(59) Lee, J. N.; Park, C.; Whitesides, G. M. Solvent Compatibility of Poly(Dimethylsiloxane)-Based Microfluidic Devices. *Anal. Chem.* **2003**, *75*, 6544−6554.
(60) Dwivedi, D.; Lepková, K.; Becker, T. Carbon Steel Corrosion: A Review of Key Surface Properties and Characterization Methods. *RSC Adv.* **2017**, *7*, 4580−4610.
(61) Dhaiveegan, P.; Elangovan, N.; Nishimura, T.; Rajendran, N. Corrosion Behavior of 316l and 304 Stainless Steels Exposed to Industrial-Marine-Urban Environment: Field Study. *RSC Adv.* **2016**, *6*, 47314−47324.
(62) Traverso, P.; Canepa, E. A Review of Studies on Corrosion of Metals and Alloys in Deep-Sea Environment. *Ocean. Eng.* **2014**, *87*, 10−15.
(63) Tesler, A. B.; Sannomiya, T.; Vaskevich, A.; Sabatani, E.; Rubinstein, I. Highly Sensitive Colorimetric Detection of Early Stage Aluminum Corrosion in Water Using Plasmonic Gold Nanoparticle Films. *Adv. Opt. Mater.* **2018**, *6*, 1800599.
(64) Sakuraba, K.; Kitano, S.; Kowalski, D.; Aoki, Y.; Habazaki, H. Slippery Liquid-Infused Porous Surfaces on Aluminum for Corrosion

https://doi.org/10.1021/acsami.2c04960
ACS Appl. Mater. Interfaces 2022, 14, 29386−29397

Protection with Improved Self-Healing Ability. *ACS Appl. Mater. Interfaces* **2021**, *13*, 45089−45096.
(65) Callow, J. A.; Callow, M. E. Biofilms. In *Antifouling Compounds*; Fusetani, N., Clare, A. S., Eds.; Springer: Berlin, Heidelberg, 2006; pp 141−169
(66) Li, T.; Zheng, Y.; Yu, L.; Chen, S. Mixotrophic Cultivation of a Chlorella Sorokiniana Strain for Enhanced Biomass and Lipid Production. *Biomass Bioenergy* **2014**, *66*, 204−213.
(67) Kreis, C. T.; Le Blay, M.; Linne, C.; Makowski, M. M.; Bäumchen, O. Adhesion of Chlamydomonas Microalgae to Surfaces Is Switchable by Light. *Nat. Phys.* **2018**, *14*, 45−49.
(68) Liu, S.; Guo, W. Anti-Biofouling and Healable Materials: Preparation, Mechanisms, and Biomedical Applications. *Adv. Funct. Mater.* **2018**, *28*, 1800596.
(69) Zhang, Y.; Ma, R.; Chu, H.; Zhou, X.; Yao, T.; Zhang, Y. Evaluation of the Performance of Different Membrane Materials for Microalgae Cultivation on Attached Biofilm Reactors. *RSC Adv.* **2022**, *12*, 1451−1459.
(70) Zhang, B.; Xu, W. Superhydrophobic, Superamphiphobic and Slips Materials as Anti-Corrosion and Anti-Biofouling Barriers. *New J. Chem.* **2021**, *45*, 15170−15179.
(71) Atthi, N.; Suwan, M.; Sangwong, N.; Pattamang, P.; Sripumkhai, W.; Meananeatra, R.; Saengdee, P.; Thongsook, O.; Ranron, N.; Pankong, K.; Uahchinkul, W.; Jeamsaksiri, W.; Supothina, S. Fabrication of Slippery Liquid-Infused Porous Surfaces for Anti-Fouling Applications. *Jpn. J. Appl. Phys.* **2021**, *60*, SCCJ04.
(72) Xiao, L.; Li, J.; Mieszkin, S.; Di Fino, A.; Clare, A. S.; Callow, M. E.; Callow, J. A.; Grunze, M.; Rosenhahn, A.; Levkin, P. A. Slippery Liquid-Infused Porous Surfaces Showing Marine Antibiofouling Properties. *ACS Appl. Mater. Interfaces* **2013**, *5*, 10074−10080.
(73) Holzinger, A.; Karsten, U. Desiccation Stress and Tolerance in Green Algae: Consequences for Ultrastructure, Physiological and Molecular Mechanisms. *Front. Plant Sci.* **2013**, *4*, 327.
(74) Stafslien, S.; Daniels, J.; Mayo, B.; Christianson, D.; Chisholm, B.; Ekin, A.; Webster, D.; Swain, G. Combinatorial Materials Research Applied to the Development of New Surface Coatings Iv. A High-Throughput Bacterial Biofilm Retention and Retraction Assay for Screening Fouling-Release Performance of Coatings. *Biofouling* **2007**, *23*, 45−54.
(75) Stafslien, S. J.; Sommer, S.; Webster, D. C.; Bodkhe, R.; Pieper, R.; Daniels, J.; Vander Wal, L.; Callow, M. C.; Callow, J. A.; Ralston, E.; Swain, G.; Brewer, L.; Wendt, D.; Dickinson, G. H.; Lim, C.-S.; Teo, S. L.-M. Comparison of Laboratory and Field Testing Performance Evaluations of Siloxane-Polyurethane Fouling-Release Marine Coatings. *Biofouling* **2016**, *32*, 949−968.
(76) Falciatore, A.; Jaubert, M.; Bouly, J.-P.; Bailleul, B.; Mock, T. Diatom Molecular Research Comes of Age: Model Species for Studying Phytoplankton Biology and Diversity. *Plant Cell* **2019**, *32*, 547−572.
(77) Chiovitti, A.; Dugdale, T. M.; Wetherbee, R. Diatom Adhesives: Molecular and Mechanical Properties. In *Biological Adhesives*; Smith, A. M., Callow, J. A., Eds.; Springer: Berlin, Heidelberg, 2006; pp 79−103
(78) Holland, R.; Dugdale, T. M.; Wetherbee, R.; Brennan, A. B.; Finlay, J. A.; Callow, J. A.; Callow, M. E. Adhesion and Motility of Fouling Diatoms on a Silicone Elastomer. *Biofouling* **2004**, *20*, 323−329.
(79) Reimann, B. E. F.; Lewin, J. M. C.; Guillard, R. R. L. Cyclotella Cryptica, a New Brackish-Water Diatom Species. *Phycologia* **1963**, *3*, 75−84.
(80) Kolle, S.; Ahanotu, O.; Meeks, A.; Stafslien, S.; Kreder, M.; Vanderwal, L.; Cohen, L.; Waltz, G.; Lim, C. S.; Slocum, D.; Maldonado-Greene, E.; Hunsucker, K.; Swain, G.; Wendt, D.; Lay-Ming Teo, S.; Aizenberg, J. *On the Mechanism of Marine Fouling-Prevention Performance of Oil-Containing Silicone Elastomers: A Comprehensive Laboratory, Field and Theoretical Study*, 2022, *available at Research Square* **2022**, *PREPRINT (Version 1)*.

https://doi.org/10.1021/acsami.2c04960
ACS Appl. Mater. Interfaces 2022, 14, 29386−29397